# Production cross sections of $^{52}$Mn in alpha-particle-induced reactions on natural vanadium

Damdinsuren Gantumur [a, b, *], Masayuki Aikawa [a, c,d], Tegshjargal Khishigjargal [b], Erdene Norov [b], Shuichiro Ebata [e], Hiromitsu Haba [f]

[a] *Graduate School of Biomedical Science and Engineering, Hokkaido University, Sapporo 060-8638, Japan*

[b] *School of Engineering and Applied Sciences, National University of Mongolia, Ulaanbaatar 14201, Mongolia*

[c] *Faculty of Science, Hokkaido University, Sapporo 060-0810, Japan*

[d] *Global Center for Biomedical Science and Engineering, Faculty of Medicine, Hokkaido University, Sapporo 060-8648, Japan*

[e] *Graduate School of Science and Engineering, Saitama University, Saitama 338-8570, Japan*

[f] *Nishina Center for Accelerator-Based Science, RIKEN, Wako 351-0198, Japan*

## Abstract

Activation cross sections of alpha-particle-induced reactions on natural vanadium were measured. The production cross sections of $^{54, 52g}$Mn, $^{51}$Cr, $^{48}$V, and $^{47, 46g}$Sc were determined up to 50 MeV. The stacked-foil activation technique and high-resolution gamma-ray spectrometry were used. The experimental results were compared with previous experimental data and theoretical calculations in the TENDL-2019 library. The physical yield of the medical radionuclide $^{52g}$Mn was derived from the measured cross sections.

## Keyword

Manganese-52; Alpha-particle irradiation; Vanadium target; Excitation function; Cross section

## 1. Introduction

The radioisotope $^{52}$Mn has the ground state $^{52g}$Mn with a half-life of $T_{1/2}$ = 5.6 d, which decays via electron capture (70.6%) and positron emission (29.4%, $\langle E_{\beta+} \rangle$ = 242 keV) processes. It has also a metastable state $^{52m}$Mn ($T_{1/2}$ = 21.1 min) that decays to the ground state $^{52g}$Mn by isomeric transition (IT) (1.8%) and to $^{52}$Cr by electron capture (1.6%) and positron emission (96.6%, $\langle E_{\beta+} \rangle$ = 1172 keV) processes according to NuDat 3.0 (National Nuclear Data Center, 2021). $^{52g}$Mn can be used in Positron Emission Tomography (PET) imaging to study biological and physiological processes with a time scale similar to its decay (Bianchi et al., 2020).

---

* Corresponding author: Damdinsuren Gantumur, damdinsuren@nds.sci.hokudai.ac.jp
Present address: Graduate School of Biomedical Science and Engineering, Hokkaido University, Sapporo 060-8638, Japan

The promising routes of $^{52}$Mn production are proton- and deuteron-induced reactions on natural chromium or enriched $^{52}$Cr targets (Tárkányi et al., 2019). Another possible production route is alpha-particle-induced reactions on natural vanadium ($^{nat}$V) targets. $^{nat}$V is a monoisotopic element, although it has two isotopes of $^{51}$V (stable, 99.75%) and $^{50}$V ($T_{1/2} = 2.1\times10^{17}$ y, 0.25%) according to NuDat 3.0 (National Nuclear Data Center, 2021). There are many previous measurements of alpha-particle-induced reactions on $^{nat}$V (Ali et al., 2018; Bindu et al., 1998; Bowman & Blann, 1969; Chowdhury et al., 1995; Dmitriev et al., 1969; Hansper et al., 1993; Iguchi et al., 1960; Ismail, 1993; Levkovski, 1991; Michel et al., 1983; Neuzil & Lindsay, 1963; Peng et al., 1999; Rama et al., 1987; Singh et al., 1993, 1995; Sonzogni et al., 1993; Vlieks et al., 1974; Vonach et al., 1983). However, their data show large uncertainties and discrepancies.

In this paper, we present results of measurement of the excitation functions of the alpha-particle-induced reactions on $^{nat}$V up to 50 MeV, with a particular focus on the $^{52g}$Mn production. Activation cross sections of several co-produced radioisotopes were also determined. The experimental results were compared with earlier studies and theoretical calculations in the TENDL-2019 library (Koning et al., 2019). The physical yield of $^{52g}$Mn was derived from the measured cross sections.

## 2. Experimental

The experiment was performed at the AVF cyclotron of the RIKEN RI Beam Factory. The stacked-foil activation technique and high-resolution gamma-ray spectrometry were used.

The target for the experiment consisted of metallic foils of $^{nat}$V (25-μm thick, 99% purity, Nilaco Corp., Japan), $^{nat}$Ti (5-μm thick, 99.6% purity, Nilaco Corp., Japan), and $^{27}$Al (5-μm thick, >99% purity, Nilaco Corp., Japan). The $^{27}$Al foils were used to catch recoiled reaction products from the $^{nat}$V and $^{nat}$Ti foils, while the $^{nat}$Ti foils were to assess beam parameters and target thicknesses by the $^{nat}$Ti(α,x)$^{51}$Cr monitor reactions. The target thicknesses were derived using measured sizes and weights of the foils. The derived thicknesses of the $^{nat}$V, $^{nat}$Ti and $^{27}$Al foils were 20.4, 2.24 and 1.22 mg/cm$^2$, respectively. The foils were then cut into 8×8 mm$^2$ to fit a target holder served as a Faraday cup. Eleven sets of V-Al-Ti-Ti-Al foils were stacked in the target holder.

The stacked target was irradiated for 30 minutes with a 50.6±0.2 MeV alpha-particle beam. The primary beam energy was measured by the time-of-flight method (Watanabe et al., 2014). The energy degradation in the stacked target was calculated using the SRIM code (Ziegler et al., 2010). The average beam intensity measured by the Faraday cup was 194 nA.

The gamma-ray spectra of each irradiated foil were measured without chemical separation by a high-resolution HPGe detector (ORTEC GEM-25185-P). The gamma-ray spectra were analyzed by the dedicated software (SEIKO EG&G Gamma Studio). The detector was calibrated by a multiple gamma-ray emitting point source consisting of $^{57,60}$Co, $^{88}$Y, $^{109}$Cd, $^{113}$Sn $^{137}$Cs, $^{139}$Ce, and $^{241}$Am. Each $^{nat}$V foil was measured together with the next $^{27}$Al catcher foil of recoiled products. Each foil was measured three times in 17 days to follow the decay of the produced radioisotopes with different half-lives. The distance between the detector and the foils was arranged to keep the dead time less than 3%.

The nuclear reaction and decay data for the gamma-ray spectrometry were taken from NuDat 3.0 (National Nuclear Data Center, 2021) and QCalc (Sonzogni & Pritychenko, 2003). Reaction and decay data for the radionuclides of interest are listed in Table 1.

Cross sections of the $^{nat}Ti(\alpha,x)^{51}Cr$ monitor reaction were derived to assess the beam parameters and target thicknesses. The gamma line at 320.08 keV ($I_\gamma$ = 9.91%) from the decay of $^{51}Cr$ ($T_{1/2}$ = 27.7025 d) was measured. Only the low energy Ti foil of each Ti-Ti foil pairs in the stack was assessed, as it was considered to be compensated for the recoiled $^{51}Cr$ reaction products. The dead time during the measurements was kept at less than 1% after a cooling time of 3 days. The derived cross sections were compared with the IAEA recommended values (Hermanne et al., 2018; Tárkányi et al., 2007) as shown in Fig. 1. Our result is consistent with the recommended values published in 2007. The measured thicknesses and beam parameters were used without any correction to derive production cross sections.

## 3. Result and discussion

The activation cross sections of $^{54,\,52g}Mn$, $^{51}Cr$, $^{48}V$, and $^{47,\,46g}Sc$ were determined for the alpha-particle-induced reactions on $^{nat}V$. The numerical data of the measured cross sections are listed in Table 2. The results are displayed in Figs. 2-7 together with the previous experimental studies and the TENDL-2019 data. The production yield of $^{52g}Mn$ deduced from the measured cross sections is shown in Fig. 8. The yield was compared with the previous experimental data (Dmitriev et al., 1969).

The median projectile energy at each foil is listed in Table 2 with the total uncertainty and energy loss in parathesis. The total energy uncertainties of 0.2-1.3 MeV were propagated from the uncertainties of the primary beam energy (±0.2 MeV) and target thickness (1%). The estimated energy loss in the $^{nat}V$ foils was 1.0-5.3 MeV. The total uncertainty of the cross sections was estimated to be 7.2-29.5%. It was derived from the square root of the quadratic summation of each component; beam intensity (5%), gamma-line intensity (<13%), detector efficiency (5%), target thickness (1%), target purity (1%), and counting statistics (0.2-28.6%).

### 3.1 The $^{nat}V(\alpha,x)^{54}Mn$ reaction

The cross sections of the $^{nat}V(\alpha,x)^{54}Mn$ reaction were derived from the gamma line at 834.848 keV ($I_\gamma$ = 99.976%) emitted with the decay of $^{54}Mn$ ($T_{1/2}$ = 312.20 d). The gamma line was measured after an average cooling time of 17 days. The result is compared with the previous studies (Ali et al., 2018; Bindu et al., 1998; Bowman & Blann, 1969; Chowdhury et al., 1995; Hansper et al., 1993; Iguchi et al., 1960; Ismail, 1993; Levkovski, 1991; Michel et al., 1983; Peng et al., 1999; Rama et al., 1987; Singh et al., 1993, 1995; Sonzogni et al., 1993; Vlieks et al., 1974; Vonach et al., 1983) and the

TENDL-2019 data (Koning et al., 2019) as shown in Fig. 2. Our data point at the lowest energy is shifted to the lower energy region because the beam was fully stopped at the corresponding foil.

The present data are consistent with the data of Ali et al. (2018), Bindu et al. (1998), Bowman & Blann (1969), Iguchi et al. (1960), Levkovski (1991), Michel et al. (1983), Peng et al. (1999), and Sonzogni et al. (1993). The partial agreement is found with the data of Chowdhury et al. (1995), Ismail (1993), Rama et al. (1987), and Singh et al. (1993, 1995) in the higher energy region. The data below 11 MeV by Hansper et al. (1993), Vlieks et al. (1974), and Vonach et al. (1983) are smaller than ours while the previous data are consistent with each other except for part of the data by Vlieks et al. (1974) at around the peak. The TENDL-2019 data show the same trend as the experimental excitation function while they underestimate above the peak.

### 3.2 The $^{nat}V(\alpha,x)^{52g}Mn$ reaction

The cross sections of the $^{nat}V(\alpha,x)^{52g}Mn$ reaction were derived. The radionuclide $^{52}Mn$ has a short-lived metastable state ($T_{1/2}$ = 21.1 min), which decays partially to the ground state $^{52g}Mn$ ($T_{1/2}$ = 5.591 d) and the stable $^{52}Cr$ soon after the end of the bombardment. The gamma line at 935.544 keV ($I_\gamma$ = 94.5%) from the decay of $^{52g}Mn$ was measured after a cooling time of 17 days. The cumulative cross sections were obtained from the net counts of the gamma peak. The derived cross sections are shown in Fig. 3 and compared with the previous studies (Bindu et al., 1998; Bowman & Blann, 1969; Chowdhury et al., 1995; Dmitriev et al., 1969; Ismail, 1993; Levkovski, 1991; Michel et al., 1983; Rama et al., 1987; Singh et al., 1993, 1995; Sonzogni et al., 1993) and the TENDL-2019 data (Koning et al., 2019).

The present cross-section data show a smooth curve and are consistent with part of the previous experimental data. The data reported by Levkovski (1991) agree with our data. The experimental data of Bindu et al. (1998), Bowman & Blann (1969), Ismail (1993), Michel et al. (1983), and Singh et al. (1995) are in partial agreement with our data. The data of Chowdhury et al. (1995), Dmitriev et al. (1969), Rama et al. (1987), Singh et al. (1993), and Sonzogni et al. (1993) are lower than ours. The peak position and amplitude of the TENDL-2019 data are different from the experimental data.

### 3.3 The $^{nat}V(\alpha,x)^{51}Cr$ reaction

Measurements of the 320.08 keV gamma line ($I_\gamma$ = 9.91%) after a cooling time longer than 17 days were used to derive the production cross sections of $^{51}Cr$ ($T_{1/2}$ = 27.7025 d). Its parent $^{51}Mn$ ($T_{1/2}$ = 46.2 min) decayed completely during the cooling time. The cumulative cross sections are shown in Fig. 4 together with the previous experimental data (Bowman & Blann, 1969; Chowdhury et al., 1995; Ismail, 1993; Levkovski, 1991; Michel et al., 1983; Singh et al., 1993, 1995; Sonzogni et al., 1993) and the TENDL-2019 data (Koning et al., 2019).

The present cross sections are consistent with the data reported by Bindu et al. (1998), Ismail

(1993), Levkovski (1991), and Singh et al. (1993, 1995). Both datasets of Bowman & Blann (1969), and Sonzogni et al. (1993) are slightly lower than ours in the higher energy region. The data reported by Michel et al. (1982) is higher than the other experimental data. The TENDL-2019 data are larger than all the experimental data above 35 MeV.

### 3.4 The $^{nat}V(\alpha,x)^{48}V$ reaction

The excitation function of the $^{nat}V(\alpha,x)^{48}V$ reaction was derived from measurements of the gamma line at 983.525 keV ($I_{\gamma}$ = 99.98%) from the $^{48}V$ decay ($T_{1/2}$ = 15.9735 d). The measurements were performed after an average cooling time of 17 days. During the cooling time, the parent nucleus $^{48}Cr$ ($T_{1/2}$ = 21.56 h) decayed to $^{48}V$. The possible contribution of $^{48}Sc$ ($T_{1/2}$ = 43.67 h) to the gamma line was negligible because another gamma line at 1037.522 keV ($I_{\gamma}$ = 97.6%) from the $^{48}Sc$ decay could not be found in the spectra. The cumulative cross sections are shown in Fig. 5 together with the experimental data studied earlier (Bindu et al., 1998; Ismail, 1993; Michel et al., 1983; Singh et al., 1993, 1995; Sonzogni et al., 1993) and the TENDL-2019 data (Koning et al., 2019).

The present data are consistent with the data of Singh et al. (1993), Sonzogni et al. (1993), and Bindu et al. (1998) within the uncertainty. The data of Ismail (1993), and Singh et al. (1995) are lower than ours while the data reported by Michel et al. (1983) are higher than the other experimental data. The TENDL-2019 data overestimate the experimental cross sections.

### 3.5 The $^{nat}V(\alpha,x)^{47}Sc$ reaction

The production cross sections of $^{47}Sc$ ($T_{1/2}$ = 3.3492 d) were derived from the gamma line at 159.381 keV ($I_{\gamma}$ = 68.3%). We used the gamma spectra recorded after a cooling time of 1 day. The formation of $^{47}Ca$ ($T_{1/2}$ = 4.536 d) was energetically possible but negligible because the gamma line at 1297.09 keV ($I_{\gamma}$ = 67%) from $^{47}Ca$ decay could not be found in the spectra. The cross sections are shown in Fig. 6 together with the previous experimental data (Bindu et al., 1998; Bowman & Blann, 1969; Ismail, 1993; Levkovski, 1991; Michel et al., 1983; Neuzil & Lindsay, 1963; Singh et al., 1993, 1995; Sonzogni et al., 1993) and the TENDL-2019 data (Koning et al., 2019).

Our result is consistent with the data of Levkovski (1991). The experimental data of Ismail (1993), and Michel et al. (1983) are in partial agreement with ours. The data of Bindu et al. (1998), Bowman & Blann (1969), Neuzil & Lindsay (1963), Singh et al. (1993, 1995), and Sonzogni et al. (1993) are lower than our data. The TENDL-2019 data underestimate the experimental values except for the data of Singh (1995).

### 3.6 The $^{nat}V(\alpha,x)^{46g}Sc$ reaction

The cross sections for the $^{46g}Sc$ production were derived by measuring the 889.277 keV gamma line ($I_{\gamma}$ = 99.984%) from the decay ($T_{1/2}$ = 83.79 d). The metastable state $^{46m}Sc$ has a short half-life

($T_{1/2}$ = 18.75 s, IT: 100%) and decayed to $^{46g}$Sc during the irradiation. The measurements of the gamma line were performed after an average cooling time of 17 days. The cumulative cross sections are shown in Fig. 7 together with the previous experimental data (Bindu et al., 1998; Bowman & Blann, 1969; Ismail, 1993; Levkovski, 1991; Michel et al., 1983; Neuzil & Lindsay, 1963; Singh et al., 1995; Sonzogni et al., 1993) and the TENDL-2019 data (Koning et al., 2019).

The data of Ismail (1993), Levkovski (1991), and Neuzil & Lindsay (1963) are nearly consistent with our data. The previous experimental data of Bindu et al. (1998), Michel et al. (1983), and Singh et al. (1993) are higher than our result. The data of Bowman & Blann (1969) and Sonzogni et al. (1993) are lower than ours. The TENDL-2019 data underestimate the experimental data other than part data of Bowman & Blann (1969).

### 3.7 The physical yield of $^{52g}$Mn

Physical thick target yield (Otuka & Takács, 2015) of $^{52g}$Mn was deduced up to 49.6 MeV from the spline fitted curve of the measured excitation function of the $^{nat}$V(α,x)$^{52g}$Mn reaction in section 3.2 and stopping powers calculated using the SRIM code (Ziegler et al., 2010). The physical yield is displayed in Fig. 8 together with the previously published experimental data (Dmitriev et al., 1969). Our result is higher than the previous data, which can be expected from the difference of the cross sections shown in Fig. 3.

## 4. Conclusion

We measured excitation functions of the alpha-particle-induced reactions on $^{nat}$V up to 50 MeV at the RIKEN AVF cyclotron. The production cross sections of $^{52g}$Mn and co-produced $^{54}$Mn, $^{51}$Cr, $^{48}$V, and $^{47, 46g}$Sc were determined. The stacked-foil activation technique and the high-resolution gamma-ray spectrometry were used for the cross-section measurements. The measured data are compared with previous experimental data and the theoretical calculations in the TENDL-2019 library. The derived excitation function of the $^{nat}$V(α,x)$^{52g}$Mn reaction is consistent with the earlier published data of Levkovski (1991). The physical yield of $^{52g}$Mn deduced from the measured cross sections is larger than the experimental data of Dmitriev et al. (1969).


## Acknowledgment

This work was carried out at RI Beam Factory operated by RIKEN Nishina Center and CNS, University of Tokyo, Japan. G. Damdinsuren was granted a scholarship by the M-JEED project (Mongolian-Japan Engineering Education Development Program, J11B16).


## Declarations of interest

None

## References


Ali, B. M., Al-Abyad, M., Seddik, U., El-Kameesy, S. U., Ditrói, F., Takács, S., & Tárkányi, F. (2018). Activation cross-section data for α-particle-induced nuclear reactions on natural vanadium for practical applications. Pramana - Journal of Physics 90, 41. https://doi.org/10.1007/s12043-018-1527-z

Bianchi, F., Marchi, C., Fuad, G., Groppi, F., Haddad, F., Magagnin, L., & Manenti, S. (2020). On the production of $^{52g}Mn$ by deuteron irradiation on natural chromium and its radionuclidic purity. Applied Radiation and Isotopes, 166, 109329. https://doi.org/10.1016/j.apradiso.2020.109329

Bindu, K. B., Mukheijee, S., & Singh, N. L. (1998). Pre-equilibrium model analysis of alpha particle induced reactions up to 80 MeV. Physica Scripta, 57, 201-206. https://doi.org/10.1088/0031-8949/57/2/007

Bowman, W. W., & Blann, M. (1969). Reactions of $^{51}V$ and $^{27}Al$ with 7-120 MeV α-particles (equilibrium and non-equilibrium statistical analyses). Nuclear Physics, Section A, 131, 513-531. https://doi.org/10.1016/0375-9474(69)90592-2

Chowdhury, D. P., Pal, S., Saha, S. K., & Gangadharan, S. (1995). Determination of cross section of α-induced nuclear reaction on natural Cr and Zr by stacked foil activation for thin layer activation analysis. Nuclear Inst. and Methods in Physics Research, B, 103, 261-266. https://doi.org/10.1016/0168-583X(95)00663-X

Dmitriev, P. P., Konstantinov, I. O., & Krasnov, N. N. (1969). Methods for producing the $Mn^{52}$ isotope. In Soviet Atomic Energy, 26, 539–541. https://doi.org/10.1007/BF01174115

Hansper, V. Y., Morton, A. J., Tims, S. G., Tingwell, C. I. W., Scott, A. F., & Sargood, D. G. (1993). Cross sections and thermonuclear reaction rates for $^{51}V(\alpha, n)^{54}Mn$ and $^{51}V(\alpha, p)^{54}Cr$. Nuclear Physics, Section A, 551, 158-172. https://doi.org/10.1016/0375-9474(93)90309-L

Hermanne, A., Ignatyuk, A. v., Capote, R., Carlson, B. v., Engle, J. W., Kellett, M. A., Kibédi, T., Kim, G., Kondev, F. G., Hussain, M., Lebeda, O., Luca, A., Nagai, Y., Naik, H., Nichols, A. L., Nortier, F. M., Suryanarayana, S. v., Takács, S., Tárkányi, F. T., & Verpelli, M. (2018). Reference Cross Sections for Charged-particle Monitor Reactions. Nuclear Data Sheets, 148, 338-382. https://doi.org/10.1016/j.nds.2018.02.009

Iguchi, A., Amano, H., & Tanaka, S. (1960). (α, n) Cross Sections for $^{48}Ti$ and $^{51}V$. Journal of the Atomic Energy Society of Japan / Atomic Energy Society of Japan, 2, 682-684. https://doi.org/10.3327/jaesj.2.682

Ismail, M. (1993). Measurement of excitation functions and mean projected recoil ranges of nuclei in α-induced reactions on F, Al, V, Co and Re nuclei. Pramana, 40, 227-251.

https://doi.org/10.1007/BF02900190

Koning, A. J., Rochman, D., Sublet, J. C., Dzysiuk, N., Fleming, M., & van der Marck, S. (2019). TENDL: Complete Nuclear Data Library for Innovative Nuclear Science and Technology. Nuclear Data Sheets, 155, 1-55. https://doi.org/10.1016/j.nds.2019.01.002

Levkovski, V. N. (1991). Middle Mass Nuclides (A=40-100) Activation Cross Sections by Medium Energy (E=10-50 MeV) Protons and Alpha-Particles. (Experiment and Systematics).

Michel, R., Brinkmann, G., & Stueck, R. (1983). Measurement and Hybrid Model Analysis of Integral Excitation Functions for α-Induced Reactions on Vanadium and Manganese. Nuclear Data for Science and Technology, 1, 599-602. https://doi.org/10.1007/978-94-009-7099-1_129

National Nuclear Data Center. (2021). Nuclear structure and decay data on-line library, Nudat 3.0 [WWW Document]. URL https://www.nndc.bnl.gov/nudat3

Neuzil, E. F., & Lindsay, R. H. (1963). Emission of $Be^7$ and competition processes at 30 to 42 MeV. Physical Review, 131, 1697-1701. https://doi.org/10.1103/PhysRev.131.1697

Otuka, N., & Takács, S. (2015). Definitions of radioisotope thick target yields. Radiochimica Acta, 103, 1-6. https://doi.org/10.1515/ract-2013-2234

Peng, X., He, F., & Long, X. (1999). Excitation functions for α-induced reactions on vanadium. Nuclear Instruments and Methods in Physics Research, Section B: Beam Interactions with Materials and Atoms, 152, 432-436. https://doi.org/10.1016/S0168-583X(99)00179-2

Rama, R. J., Mohan Rao, A. v., Mukherjee, S., Upadhyay, R., Singh, N. L., Agarwal, S., Chaturvedi, L., & Singh, P. P. (1987). Non-equilibrium effects in alpha-particle-induced reactions in light, medium and heavy nuclei up to 120 MeV. Journal of Physics G: Nuclear Physics, 13, 535-542. https://doi.org/10.1088/0305-4616/13/4/017

Singh, N. L., Agarwal, S., & Rao, J. R. (1993). Excitation function for α-particle-induced reactions in light-mass nuclei. Canadian Journal of Physics, 71, 115-121. https://doi.org/10.1139/p93-017

Singh, N. L., Mukherjee, S., Mohan Rao, A. v., Chaturvedi, L., & Singh, P. P. (1995). Effects of pre-equilibrium nucleon emission on excitation functions of various reactions in vanadium induced by alpha particles. Journal of Physics G: Nuclear and Particle Physics, 21, 399-410. https://doi.org/10.1088/0954-3899/21/3/014

Sonzogni, A. A., Romo, A. S. M. A., Mosca, H. O., & Nassiff, S. J. (1993). Alpha and deuteron induced reactions on vanadium. Journal of Radioanalytical and Nuclear Chemistry Articles, 170, 143–156. https://doi.org/10.1007/BF02134585

Sonzogni, A., & Pritychenko, B. (2003). Q-value Calculator (QCalc). NNDC, Brookhaven National Laboratory [WWW Document]. URL https://www.nndc.bnl.gov/qcalc/

Tárkányi, F. T., Ignatyuk, A. v., Hermanne, A., Capote, R., Carlson, B. v., Engle, J. W., Kellett, M. A., Kibédi, T., Kim, G. N., Kondev, F. G., Hussain, M., Lebeda, O., Luca, A., Nagai, Y., Naik, H., Nichols, A. L., Nortier, F. M., Suryanarayana, S. v., Takács, S., & Verpelli, M. (2019). Recommended nuclear data for medical radioisotope production: diagnostic positron emitters. Journal of Radioanalytical and Nuclear Chemistry, 319, 533–666. https://doi.org/10.1007/s10967-018-6380-5

Tárkányi, F, Takács S, Gul K, Hermanne A, Mustafa M.G, Nortier M, Obložinský P, Qaim S.M, Scholten B, Shubin Y.N, & Yousiang Z. (2007). Charged particle cross-section database for medical radioisotope production (updated version). IAEA-TECDOC-1211 [WWW Document]. URL https://www-nds.iaea.org/medical/medical-old/monitor_reactions.html

Vlieks, A. E., Morgan, J. F., & Blatt, S. L. (1974). Total cross sections for some (α, n) and (α, p) reactions in medium-weight nuclei. Nuclear Physics, Section A, 224, 492-502. https://doi.org/10.1016/0375-9474(74)90551-X

Vonach, H., Haight, R. C., & Winkler, G. (1983). (α, n) and total α-reaction cross sections for $^{48}$Ti and $^{51}$V. Physical Review C, 28, 2278-2285. https://doi.org/10.1103/PhysRevC.28.2278

Watanabe, T., Fujimaki, M., Fukunishi, N., Imao, H., Kamigaito, O., Kase, M., Komiyama, M., Sakamoto, N., Suda, K., Wakasugi, M., & Yamada, K. (2014). Beam energy and longitudinal beam profile measurement system at the RIBF. IPAC 2014: Proceedings of the 5th International Particle Accelerator Conference, 3566-3568. doi:10.18429/JACoW-IPAC2014-THPME136

Ziegler, J. F., Ziegler, M. D., & Biersack, J. P. (2010). SRIM - The stopping and range of ions in matter (2010). Nuclear Instruments and Methods in Physics Research, Section B: Beam Interactions with Materials and Atoms, 268, 1818-1823. https://doi.org/10.1016/j.nimb.2010.02.091

Tables

Table 1. Reactions and decay data of reaction products.

| Nuclide | Half-life | Decay mode (%) | $E_\gamma$ (keV) | $I_\gamma$ (%) | Contributing reactions | Q-value (MeV) |
|---|---|---|---|---|---|---|
| $^{54}Mn$ | 312.20 d | ε (100) | **834.848** | 99.976(10) | $^{50}V(\alpha, \gamma)^{54}Mn$ | 8.8 |
| | | | | | $^{51}V(\alpha, n)^{54}Mn$ | -2.3 |
| $^{52g}Mn$ | 5.591 d | $\varepsilon + \beta^+$ (100) | 744.233 | 90(12) | $^{50}V(\alpha, 2n)^{52}Mn$ | -12.2 |
| | | | **935.544** | 94.5(13) | $^{51}V(\alpha, 3n)^{52}Mn$ | -23.3 |
| | | | 1434.092 | 100(14) | | |
| $^{51}Cr$ | 27.7025 d | ε (100) | **320.0824** | 9.91(10) | $^{50}V(\alpha, t)^{51}Cr$ | -10.3 |
| | | | | | $^{51}V(\alpha, tn)^{51}Cr$ | -21.3 |
| $^{51}Mn$ | 46.2 m | $\varepsilon + \beta^+$ (100) | 511.0 | 194.18(6) | $^{50}V(\alpha, 3n)^{51}Mn$ | -22.8 |
| | | | 749.07 | 0.265 | $^{51}V(\alpha, 4n)^{51}Mn$ | -33.8 |
| $^{48}V$ | 15.9735 d | $\varepsilon + \beta^+$ (100) | **983.525** | 99.98(4) | $^{50}V(\alpha, \alpha 2n)^{48}V$ | -20.9 |
| | | | 1312.106 | 98.2(3) | $^{51}V(\alpha, \alpha 3n)^{48}V$ | -31.9 |
| $^{48}Sc$ | 43.67 h | $\beta^-$ (100) | 983.526 | 100.1(6) | $^{50}V(\alpha, \alpha 2p)^{48}Sc$ | -19.3 |
| | | | **1037.522** | 97.6(7) | $^{51}V(\alpha, \alpha ^3He)^{48}Sc$ | -22.6 |
| | | | 1312.12 | 100.1(7) | | |
| $^{48}Cr$ | 21.56 h | ε (100) | 112.31 | 96(20) | $^{50}V(\alpha, t3n)^{48}Cr$ | -43.1 |
| | | | 308.24 | 100 | | |
| $^{47}Sc$ | 3.3492 d | $\beta^-$ (100) | **159.381** | 68.3(4) | $^{50}V(\alpha, \alpha ^3He)^{47}Sc$ | -10.3 |
| | | | | | $^{51}V(\alpha, 2\alpha)^{47}Sc$ | -19.8 |
| $^{47}Ca$ | 4.536 d | $\beta^-$ (100) | 807.86 | 5.9(12) | $^{50}V(\alpha, \alpha 3p)^{47}Ca$ | -28.7 |
| | | | **1297.09** | 67 | $^{51}V(\alpha, \alpha p ^3He)^{47}Ca$ | -32.1 |
| $^{46g}Sc$ | 83.79 d | $\beta^-$ (100) | **889.277** | 99.984(10) | $^{50}V(\alpha, 2\alpha)^{46}Sc$ | -9.9 |
| | | | 1120.545 | 99.987(10) | $^{51}V(\alpha, 2\alpha n)^{46}Sc$ | -20.1 |
| $^{51}Cr$ | 27.7025 d | ε (100) | **320.0824** | 9.91(10) | $^{nat}Ti(\alpha, x)^{51}Cr$ | |

Table 2. Measured production cross sections (mb)

| Energy (MeV) | $^{54}Mn$ | $^{52g}Mn$(cum) | $^{51}Cr$(cum) | $^{48}V$(cum) | $^{47}Sc$ | $^{46g}Sc$(cum) |
|---|---|---|---|---|---|---|
| 49.6±0.2 (±1.0) | 6.09±0.59 | 145±10 | 296±22 | 9.69±0.70 | 3.89±0.31 | 12.1±0.9 |
| 46.8±0.2 (±1.1) | 6.99±1.13 | 190±14 | 194±14 | 2.14±0.20 | 4.17±0.35 | 7.23±0.63 |
| 43.8±0.2 (±1.1) | 8.89±1.31 | 230±17 | 95.5±7.1 | 0.507±0.108 | 4.80±0.39 | 3.18±0.40 |
| 40.7±0.3 (±1.2) | 11.9±1.5 | 259±19 | 33.8±2.8 | | 4.49±0.37 | |
| 37.4±0.3 (±1.2) | 13.0±1.5 | 239±17 | 9.68±1.38 | | 2.66±0.26 | |
| 33.9±0.3 (±1.3) | 16.6±1.6 | 172±12 | 4.73±1.06 | | 1.45±0.20 | |
| 30.1±0.4 (±1.5) | 25.5±2.0 | 59.2±4.3 | 2.11±0.62 | | 0.433±0.102 | |
| 25.8±0.5 (±1.6) | 47.0±3.5 | 2.03±0.16 | | | 0.0267±0.0027 | |
| 21.0±0.6 (±1.9) | 150±11 | 0.889±0.081 | | | | |
| 15.1±0.8 (±2.4) | 554±40 | 0.187±0.030 | | | | |
| 6.5±1.8 (±4.1) | 111±8 | | | | | |

Figure captions

Fig. 1. Excitation function of the $^{nat}Ti(\alpha,x)^{51}Cr$ monitor reaction with the recommended values (Hermanne et al., 2018; Tárkányi et al., 2007).

Fig. 2. Excitation function of the $^{nat}V(\alpha,x)^{54}Mn$ reaction.

Fig. 3. Excitation function of the $^{nat}V(\alpha,x)^{52g}Mn$ cumulative reaction.

Fig. 4. Excitation function of the $^{nat}V(\alpha,x)^{51}Cr$ cumulative reaction.

Fig. 5. Excitation function of the $^{nat}V(\alpha,x)^{48}V$ cumulative reaction.

Fig. 6. Excitation function of the $^{nat}V(\alpha,x)^{47}Sc$ reaction.

Fig. 7. Excitation function of the $^{nat}V(\alpha,x)^{46g}Sc$ cumulative reaction.

Fig. 8. Physical yield of $^{52g}Mn$ in the alpha-particle-induced reaction on $^{nat}V$.

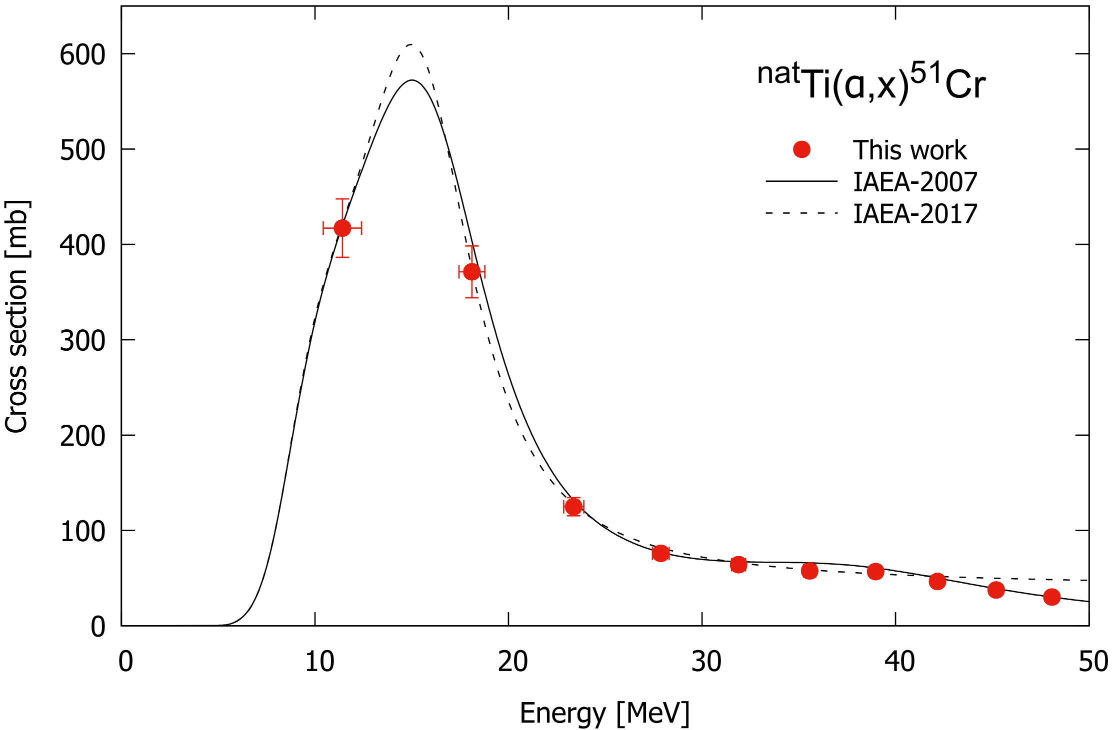

natTi(α,x)51Cr
This work
IAEA-2007
IAEA-2017
Cross section [mb]
Energy [MeV]
0
100
200
300
400
500
600
0
10
20
30
40
50

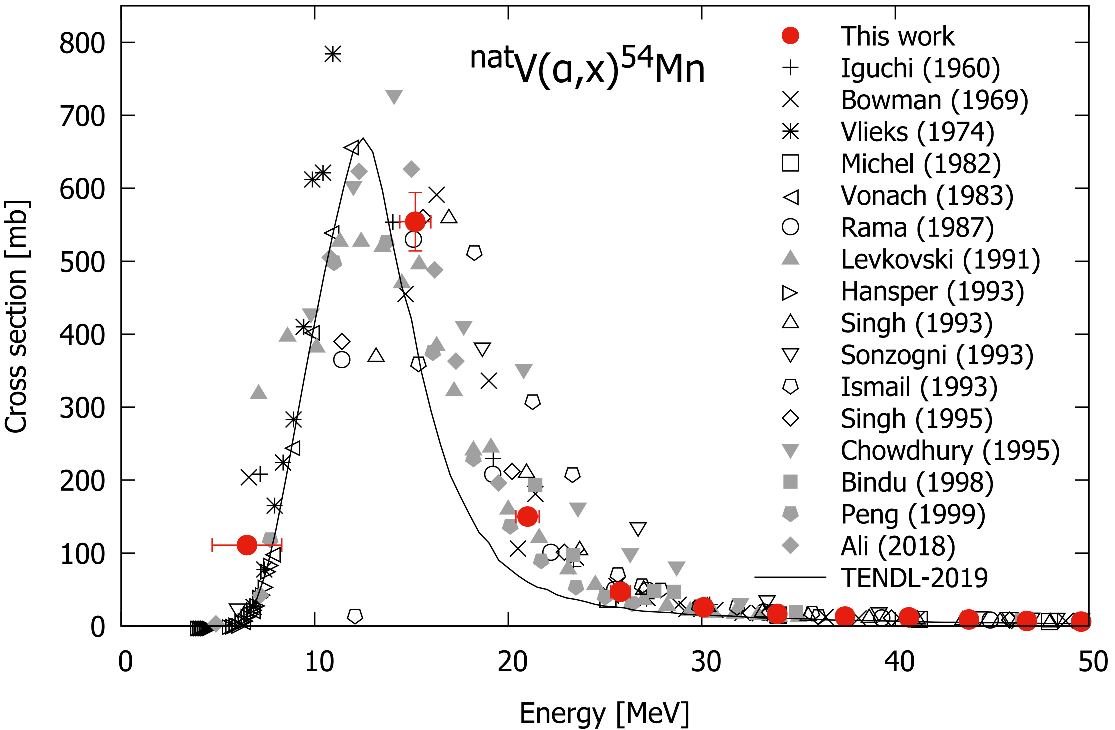

natV(α,x)54Mn
Cross section [mb]
Energy [MeV]
0
100
200
300
400
500
600
700
800
0
10
20
30
40
50
This work
Iguchi (1960)
Bowman (1969)
Vlieks (1974)
Michel (1982)
Vonach (1983)
Rama (1987)
Levkovski (1991)
Hansper (1993)
Singh (1993)
Sonzogni (1993)
Ismail (1993)
Singh (1995)
Chowdhury (1995)
Bindu (1998)
Peng (1999)
Ali (2018)
TENDL-2019

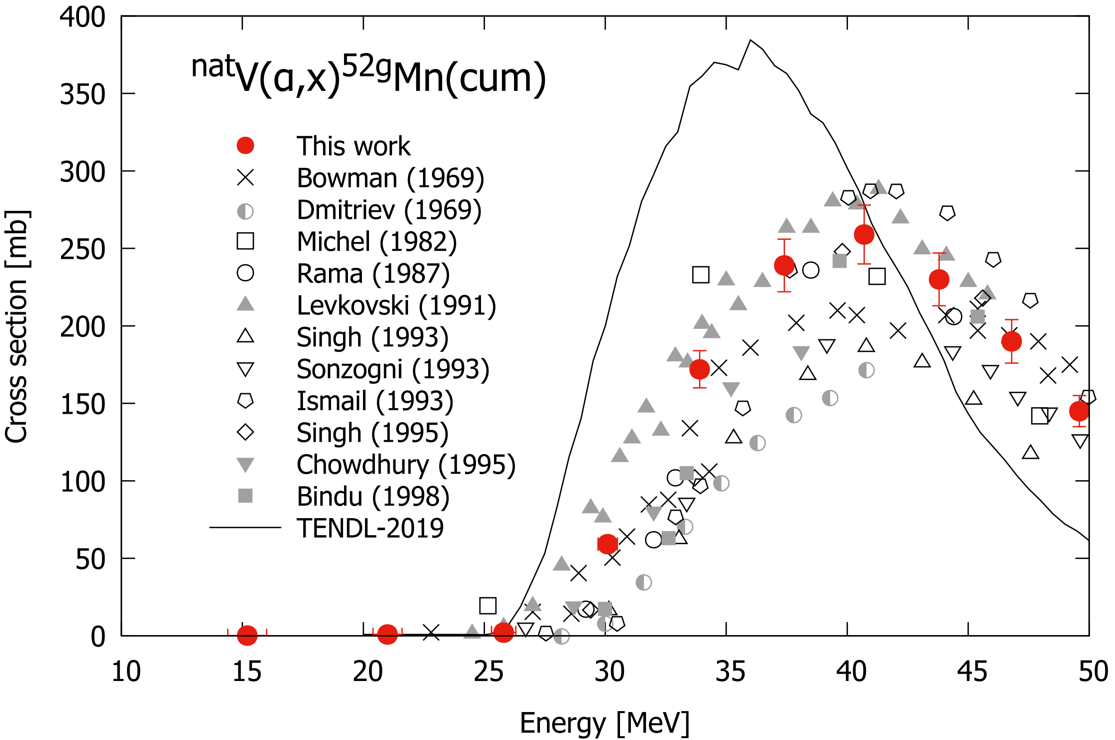

natV(α,x)52gMn(cum)
This work
Bowman (1969)
Dmitriev (1969)
Michel (1982)
Rama (1987)
Levkovski (1991)
Singh (1993)
Sonzogni (1993)
Ismail (1993)
Singh (1995)
Chowdhury (1995)
Bindu (1998)
TENDL-2019
Cross section [mb]
Energy [MeV]
0
50
100
150
200
250
300
350
400
10
15
20
25
30
35
40
45
50

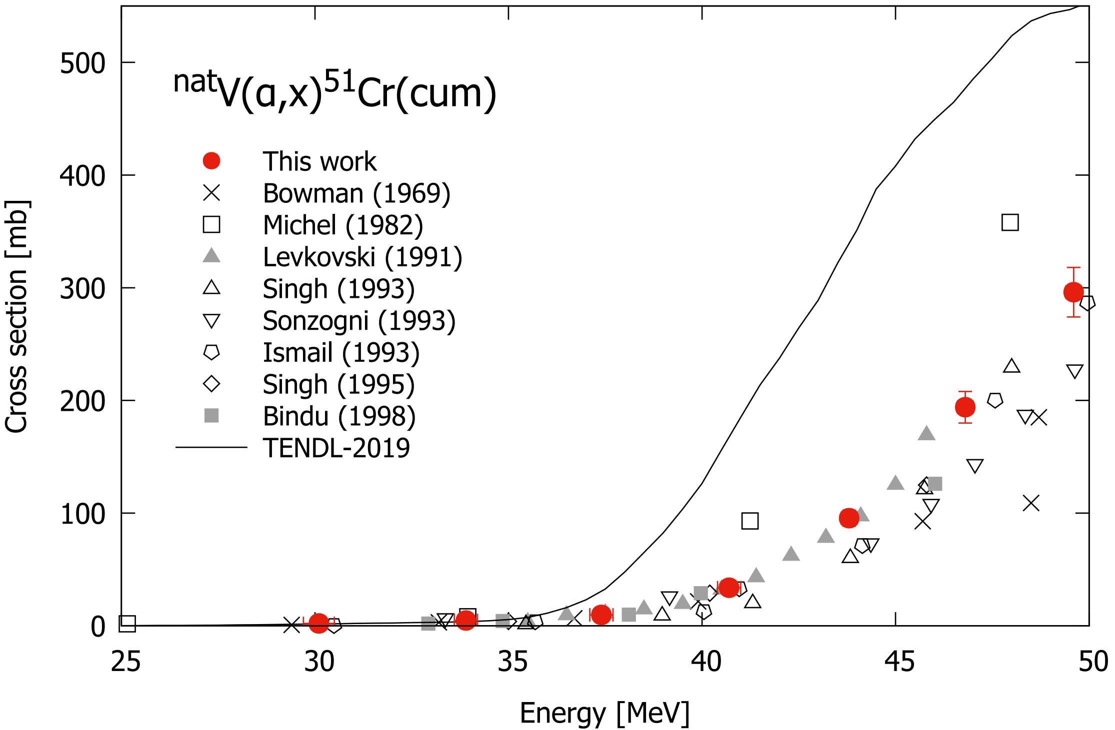

$^{nat}V(\alpha,x)^{51}Cr(cum)$
This work
Bowman (1969)
Michel (1982)
Levkovski (1991)
Singh (1993)
Sonzogni (1993)
Ismail (1993)
Singh (1995)
Bindu (1998)
TENDL-2019
Cross section [mb]
Energy [MeV]
0
100
200
300
400
500
25
30
35
40
45
50

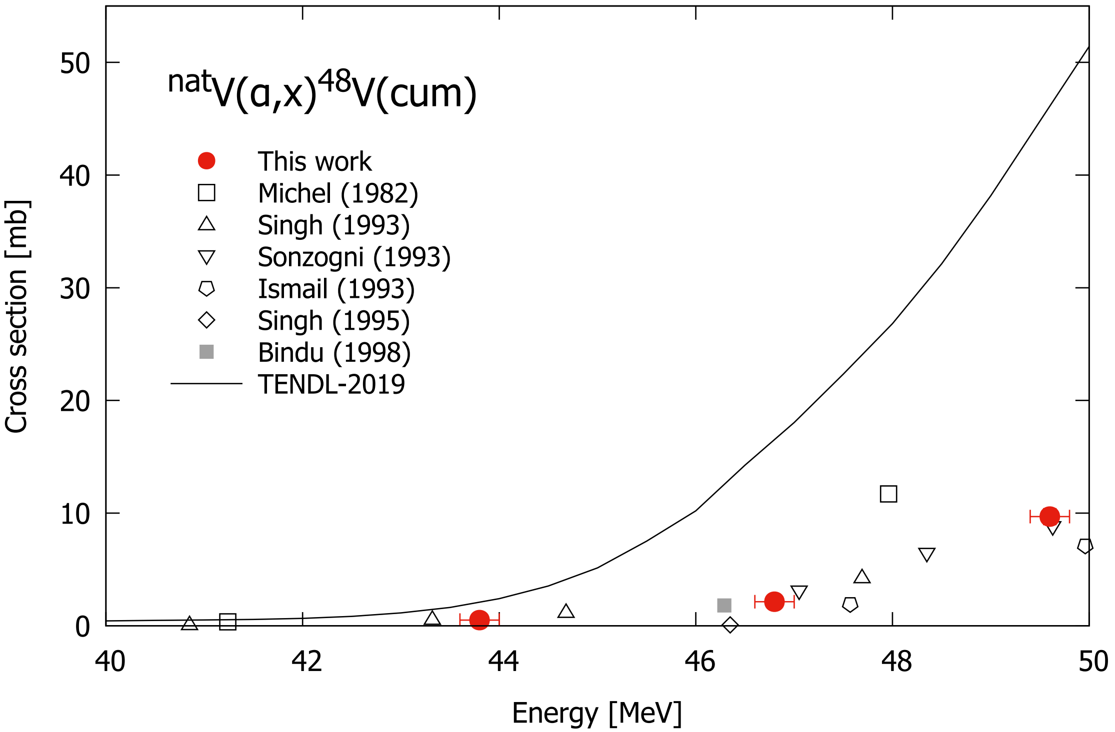

natV(α,x)48V(cum)
This work
Michel (1982)
Singh (1993)
Sonzogni (1993)
Ismail (1993)
Singh (1995)
Bindu (1998)
TENDL-2019
Cross section [mb]
Energy [MeV]
0
10
20
30
40
50
40
42
44
46
48
50

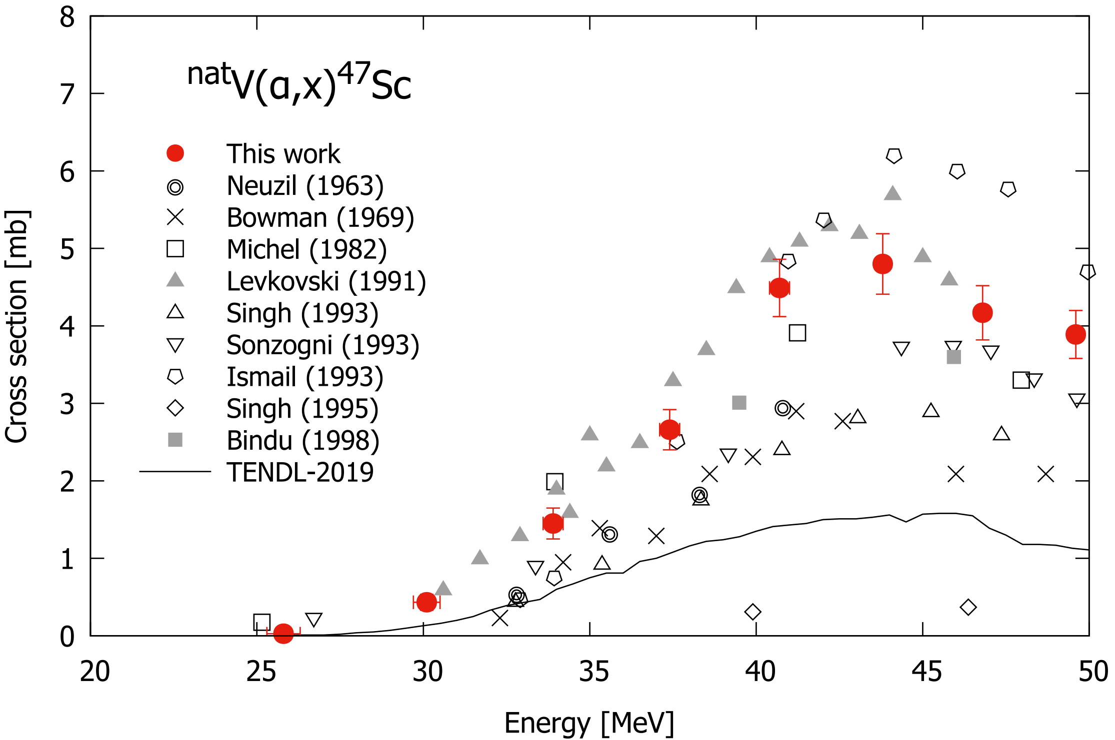

$^{nat}V(\alpha,x)^{47}Sc$
This work
Neuzil (1963)
Bowman (1969)
Michel (1982)
Levkovski (1991)
Singh (1993)
Sonzogni (1993)
Ismail (1993)
Singh (1995)
Bindu (1998)
TENDL-2019
Cross section [mb]
Energy [MeV]
0
1
2
3
4
5
6
7
8
20
25
30
35
40
45
50

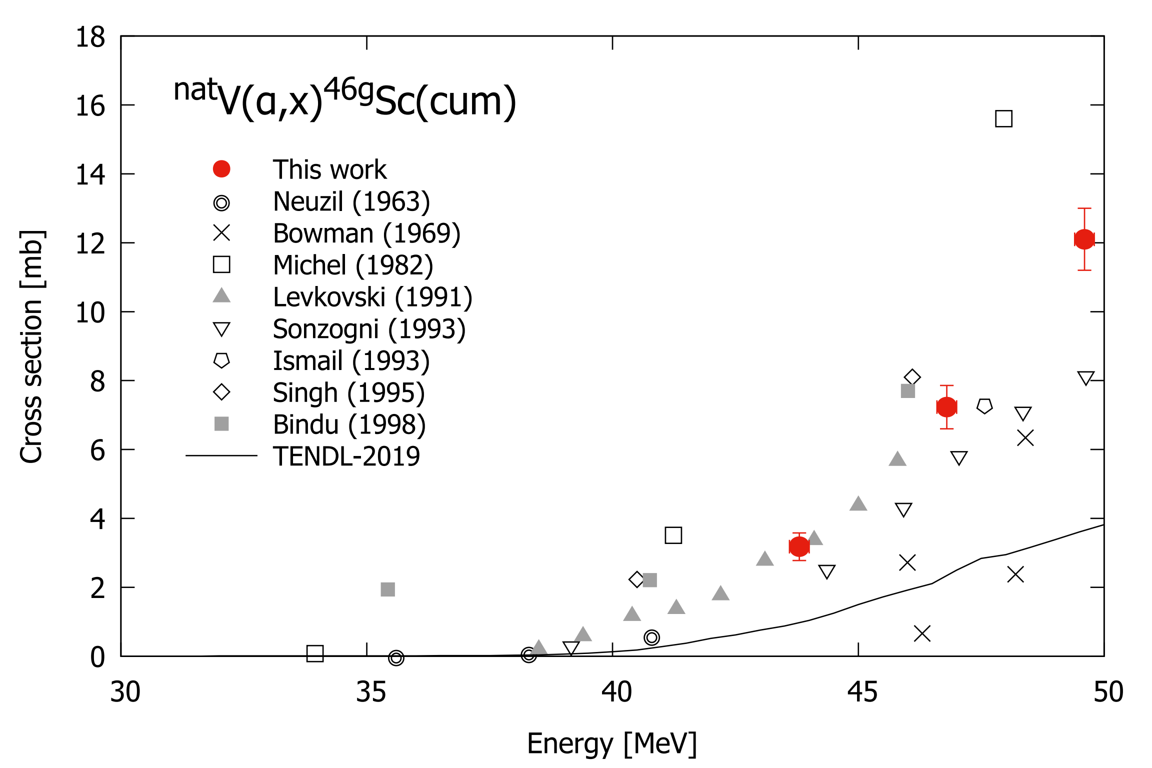

$^{nat}V(\alpha,x)^{46g}Sc(cum)$
This work
Neuzil (1963)
Bowman (1969)
Michel (1982)
Levkovski (1991)
Sonzogni (1993)
Ismail (1993)
Singh (1995)
Bindu (1998)
TENDL-2019
Cross section [mb]
Energy [MeV]
0
2
4
6
8
10
12
14
16
18
30
35
40
45
50

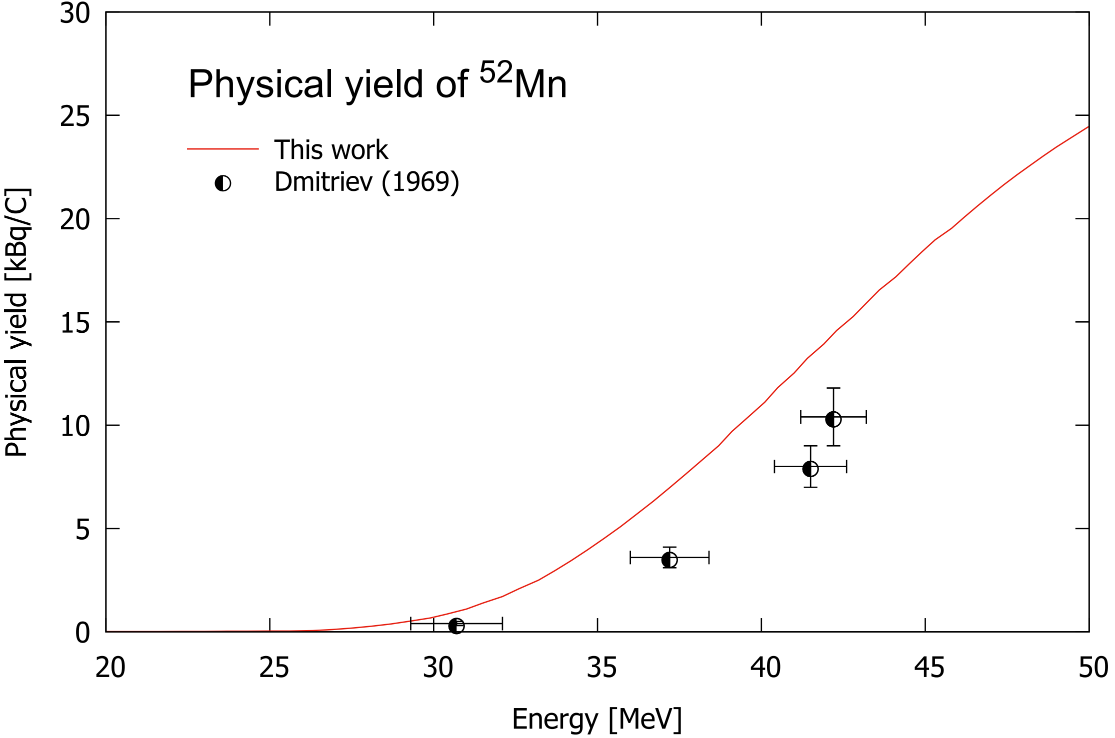
Physical yield of $^{52}$Mn
This work
Dmitriev (1969)
Physical yield [kBq/C]
Energy [MeV]
0
5
10
15
20
25
30
20
25
30
35
40
45
50